BASIC SCIENCE

Nanomedicine: Nanotechnology, Biology, and Medicine
14 (2018) 2329–2339

Research Article

nanomedjournal.com

Investigation into the pulmonary inflammopathology of exposure to nickel oxide nanoparticles in mice

Kuan-Jen Bai, MD, PhD[a,b,c,1], Kai-Jen Chuang, PhD[d,e,1], Jen-Kun Chen, PhD[f], His-En Hua, MSc[d], Yen-Ling Shen, MSc[d], Wei-Neng Liao, MSc[f], Chii-Hong Lee, MD[g], Kuan-Yuan Chen, MD[h], Kang-Yun Lee, MD, PhD[b,h], Ta-Chih Hsiao, PhD[i], Chih-Hong Pan, PhD[j,k], Kin-Fai Ho, PhD[l,m], Hsiao-Chi Chuang, PhD[a,b,h,*]

[a]*School of Respiratory Therapy, College of Medicine, Taipei Medical University, Taipei, Taiwan*
[b]*Department of Internal Medicine, School of Medicine, College of Medicine, Taipei Medical University, Taipei, Taiwan*
[c]*Division of Pulmonary Medicine, Department of Internal Medicine, Wan Fang Hospital, Taipei Medical University, Taipei, Taiwan*
[d]*School of Public Health, College of Public Health, Taipei Medical University, Taipei, Taiwan*
[e]*Department of Public Health, School of Medicine, College of Medicine, Taipei Medical University, Taipei, Taiwan*
[f]*Institute of Biomedical Engineering & Nanomedicine, National Health Research Institutes, Miaoli, Taiwan*
[g]*Department of Pathology, Shuang Ho Hospital, Taipei Medical University, New Taipei City, Taiwan*
[h]*Division of Pulmonary Medicine, Department of Internal Medicine, Shuang Ho Hospital, Taipei Medical University, New Taipei City, Taiwan*
[i]*Graduate Institute of Environmental Engineering, National Central University, Taoyuan, Taiwan*
[j]*Institute of Occupational Safety and Health, Council of Labor Affairs, Executive Yuan, New Taipei City, Taiwan*
[k]*School of Public Health, National Defense Medical Center, Taipei, Taiwan*
[l]*Jockey Club School of Public Health and Primary Care, The Chinese University of Hong Kong, Hong Kong*
[m]*Shenzhen Municipal Key Laboratory for Health Risk Analysis, Shenzhen Research Institute, The Chinese University of Hong Kong, Shenzhen, China*

Received 2 June 2017; accepted 7 October 2017

Abstract

We investigated the effects of nickel oxide nanoparticles (NiONPs) on the pulmonary inflammopathology. NiONPs were intratracheally installed into mice, and lung injury and inflammation were evaluated between 1 and 28 days. NiONPs caused significant increases in LDH, total protein, and IL-6 and a decrease in IL-10 in the BALF and increases in 8-OHdG and caspase-3 in lung tissues at 24 h. Airway inflammation was present in a dose-dependent manner from the upper to lower airways at 24 h of exposure as analyzed by SPECT. Lung parenchyma inflammation and small airway inflammation were observed by CT after NiONP exposure. 8-OHdG in lung tissues had increased with formation of fibrosis at 28 days. Focal adhesion was the most important pathways identified at 24 h as determined by protemics, whereas glutathione metabolism was the most important identified at 28 days. Our results demonstrated the pulmonary inflammopathology caused by NiONPs based on image-to-biochemical approaches.

Key words: Chest computed tomography; Fibrosis; Oxidative stress; Proteomics; Single-photon emission computed tomography

Abbreviations: 8-OHdG, 8-hydroxy-2′-deoxyguanosine; ANOVA, analysis of variance; BALF, bronchoalveolar lavage fluid; BET, Brunauer–Emmett–Teller; CT, computed tomography; DAVID, Database for Annotation Visualization and Integrated Discovery; EDX, energy-dispersive x-*ray*; FBS, fetal bovine serum; FE-SEM, field emission-scanning electron microscopy; FBP, filtered back projection; H&E, hematoxylin and eosin; HCD, high-energy collision dissociation; IT, intratracheal; iTRAQ, isobaric tags for relative and absolute quantitation; LC–MS/MS, liquid chromatography–tandem mass spectroscopy; NiONPs, nickel oxide nanoparticles; OSHA, Occupational Safety and Health Administration; PBS, phosphate-buffered saline; SPECT, single-photon emission computed tomography; SD, standard deviation.

Conflict of interest: The authors declare that they have no conflicts of interest.

This work was supported by the Institute of Occupational Safety and Health, Taiwan Council of Labor Affairs (IOSH102-M321 and IOSH103-M312), Taipei Medical University–Wan Fang Hospital (106TMU-WFH-03) and the Ministry of Science and Technology of Taiwan (104-2621-M-038-002-MY3 and 105-2633-B-038-001). Authors are grateful for the partial support from Animal Molecular Imaging Core Facility in Taiwan National Health Research Institutes.

*Corresponding author at: Taiwan CardioPulmonary Research (T-CPR) Group, School of Respiratory Therapy, College of Medicine, Taipei Medical University, Taipei, Taiwan.

E-mail address: r92841005@ntu.edu.tw (H.-C. Chuang).

[1] These authors contributed equally to the study.

https://doi.org/10.1016/j.nano.2017.10.003
1549-9634/

Inhalation of nickel-based compounds is recognized as an occupational and environmental hazard, associated with the development of pulmonary inflammation, fibrosis, and cancer.[1] The carcinogenicity of nickel-based compounds was also previously reported. For example, high-temperature green nickel oxide is classified as a "human carcinogen via inhalation exposure" (group 1A).[2] Nickel particles are classified as "possibly carcinogenic" (group 2B).[3] Recently, exposure to nickel-based compounds has raised concerns again due to the expanding production of nickel nanomaterials.[4] Nickel oxide nanoparticles (NiONPs), for example, are manufactured for numerous applications, including ceramics, sensors, paint formulations, catalysts, and storage batteries.[5] Other major occupational emission sources of NiONPs are from refining, electroplating, alloy production, and welding in workplaces.[1] The emission and application of NiONPs have led to increasing risks of pulmonary exposure; however, the effects of NiONP exposure on human health remain unclear.

The lungs are the major portal of entry for particles and as such, a critical organ for whole-body defense, by clearing deposited particles. The lung anatomy plays an important role in removing most inhaled particles. The extent to which particles are deposited and remain in the airway is a function of the flow rate, penetration, and clearance mechanisms.[6] Particles of <10 μm in size are able to penetrate into the thoracic region.[7] As the increasing number of bifurcations in the tracheobronchial region leads to a drop in air velocity, particles with sizes ranging 1-8 μm impact the mucus and are then removed via mucociliary clearance;[6] a portion of particles is also removed by slow clearance by transportation of macrophages to cilia. Particles of <0.5 μm can enter and accumulate in the alveolar zone of the distal respiratory tract and may be captured by macrophages or even translocated into the circulation.[6,8] Deposited particles in the lungs can provoke low-grade alveolar inflammation with a secondary systemic inflammatory response, resulting in pulmonary and cardiovascular exacerbation in susceptible individuals.[9] Pulmonary exposure to NiONPs was reported to induce oxidative–inflammatory responses;[10,11] however, the dose-dependent and time-dependent progression of the inflammopathology in the lungs remains unknown.

Inflammatory responses are usually protective and beneficial, but also have the potential to cause injury to the lungs.[12] Inflammatory responses repair, restore, and if necessary, remodel injured tissues. Inflammation resulting from an internal and/or external stimulus is associated with local vessel dilation, capillaries becoming leaky, and airway smooth muscles constricting. When these occur, fluid, proteins, and phagocytic cells move into the injured region. The inflammatory response triggers the migration and activation of both resident and circulating inflammatory cells, as well as the production of cytokines and growth factors. This initial recruitment of inflammatory cells into alveolar spaces is brought about by chemoattractant agents derived from the injured lung tissue. NiONPs are able to induce pulmonary inflammation, granulomas, and interstitial fibrosis after inhalation.[13,14] Inflammatory cells and cytokines play essential roles in regulating the early inflammatory response and lung injury after exposure to NiONPs. Although the proinflammatory responses to NiONPs were previously studied, acute and subacute biological responses and underlying pathways require further investigation.

Isobaric tags for relative and absolute quantitation (iTRAQ), a proteomics approach, is able to quantitatively assess protein expressions, which increases throughput as well as reducing experimental error.[15] Application of liquid chromatography–tandem mass spectroscopy (LC–MS/MS) with iTRAQ approaches is able to provide the underlying mechanisms in inhalation toxicology. To adequately characterize the pulmonary inflammopathology after exposure to NiONPs, comprehensive approaches were used in the present study, including image analyses, biochemistry, and proteomics. The objectives of this study were to: (1) determine the acute (24 h) and subacute (28 days) pulmonary responses after exposure to NiONPs; (2) investigate the progression of pulmonary inflammation and pathology over 28 days of exposure; and (3) observe expressions of lung proteins and underlying pathways between acute and subacute pulmonary effects after NiONP exposure.

Methods

NiONP preparation and reagent sources

NiONPs were obtained from Nanostructured & Amorphous Materials (Houston, TX, USA). NiONPs were thoroughly dispersed in phosphate-buffered saline (PBS) supplemented with 5% fetal bovine serum (FBS). The medium was prepared at a final concentration of 20 μg/ml after 30 min of sonication for physicochemical characterization. All of the other reagents were obtained from Sigma (St. Louis, MO, USA), unless otherwise explicitly stated.

Field emission-scanning electron microscopy (FE-SEM) and energy-dispersive x-ray (EDX) microanalysis

The physicochemistry of NiONPs (raw powder and prepared in 5% FBS-containing medium) was investigated using an FE-SEM (JEOL JSM-6500F, Chiyoda, Tokyo, Japan) and an EDX microanalytical instrument, according to our previous report.[16] Briefly, NiONPs were allowed to adhere to 12-mm carbon adhesive tabs on 13-mm aluminum SEM stubs following air-drying. The stubs were subsequently coated with platinum (Pt) to an average thickness of 10 nm by a sputter coater. FE-SEM images were obtained at an accelerating voltage of 15 kV with $\times 10^5$ resolution. The EDX Genesis Microanalysis System was used to determine elements of NiONPs.

Specific surface area and endotoxin

The specific surface area of NiONPs was measured by nitrogen adsorption at −196 °C using a Tristar 3020 gas adsorption analyzer (Micromeritics; Norcross, GA, USA), according to the Brunauer–Emmett–Teller (BET) method. The amount of endotoxin in the particles was determined using a Pierce LAL Chromogenic Endotoxin Quantitation Kit (Rockford, IL, USA), according to the manufacturers' instructions.

Hydrodynamic diameter and zeta potential

To determine the physical characteristics of NiONPs when suspended in a 5% FBS-containing solution, hydrodynamic

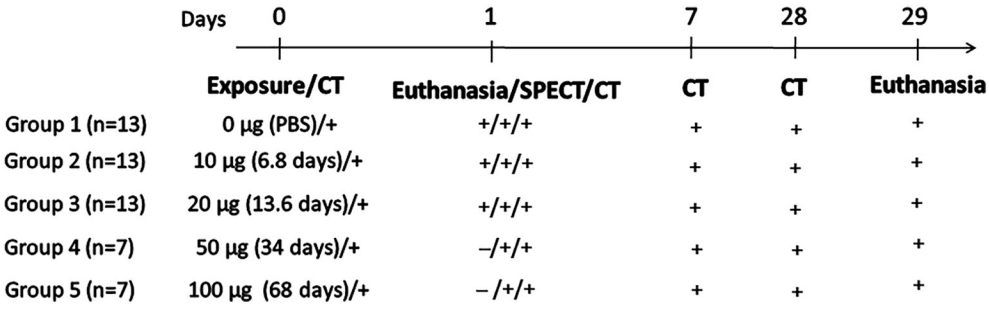

Figure 1. Overview of the experimental designs for nickel oxide nanoparticle (NiONP) exposure in female BALB/c mice. NiONPs were intratracheally instilled in mice at various concentrations (0, 10, 20, 50, and 100 μg/mouse), and lung injury and inflammation were evaluated at various time-points between 24 h and 28 days. SPECT was used to evaluate inflammatory responses in the lungs at 24 h of exposure. Chest CT was conducted to observe abnormities on days 0, 1, 7, and 28. On day 1 (24 h) and 29, mice were euthanized (n = 6 per group).

diameters and zeta potential were determined with a Malvern Zetasizer Nano-ZS (Malvern Instruments, Worcestershire, UK).

Animals

Six-week-old female BALB/c mice were obtained from BiOLASCO (Taipei, Taiwan). Mice were maintained at 22 ± 2 °C and 55% ± 10% relative humidity with a 12:12-h light/dark cycle, housed in plastic cages, and provided with Lab Diet 5001 (PMI Nutrition International, St. Louis, MO, USA) and water ad libitum during acclimatization, pre-exposure, and post-exposure. Animal experiments were approved and performed in compliance with the animal and ethics review committee of the Laboratory Animal Center at the National Health Research Institute (Miaoli, Taiwan).

Experimental design

The experimental design is shown in Figure 1. Mice were randomly divided into five groups for exposure to NiONPs at various mass concentrations. On day 0 before pulmonary exposure, a mouse in each group was randomly selected for chest computed tomography (CT) on days 1, 7, and 28 (n = 6 per group). On day 0, mice received an intratracheal (IT) instillation of 0, 10, 20, 50, or 100 μg NiONPs in 50 μL PBS with 5% FBS per mouse under light anesthesia induced by 2% isoflurane vapor (2 ml/min) using a rodent anesthesia machine (Northern Vaporiser, Skipton, UK). On day 1, one mouse was randomly selected from each group for the single-photon emission CT (SPECT) analysis. The mouse used for the SPECT analysis (n = 1 per group) was not used for any further experiments due to radiation exposure. On day 1, six mice per group were randomly euthanized to determine the acute pulmonary response (24-h follow-up), and bronchoalveolar lavage fluid (BALF) and lungs were collected. On day 29, the mice were euthanized (n = 6 per group), and BALF and organs were collected. For BALF sample collection, 1 ml of PBS was used to lavage the lungs followed by centrifugation at 1500 ×g for 5 min at 4 °C.[16] Lung tissues were snap-frozen or fixed in 4% (m/v) paraformaldehyde in PBS for the histological analyses. The doses of exposure applied in the present study are relevant to human exposure scenarios according to a previous method.[17] The mass concentrations applied in the present study were relevant to occupational exposure scenarios in humans:[18] the alveolar surface area, breathing frequency (30 times/min), lung deposition rate (30%), working day ventilation of 10 m^3,[19] and the Occupational Safety and Health Administration (OSHA) nickel permissible exposure limit of 1 mg/m^3.[20] Human-equivalent mass concentrations were achieved at 6.8 days for 10 μg, 13.6 days for 20 μg, 34 days for 50 μg, and 68 days for 100 μg in a NiONP-contaminated occupational environment. For acute health effects in mice, we selected 20 μg as the highest concentration for IT administration, because (1) 20 μg of NiONPs was able to induce significant particle toxicity in the lungs and (2) this dose was relevant to 6.8 days of a human-equivalent mass concentration.

SPECT analysis

SPECT was conducted with a preclinical tri-modality imaging system (FLEX Triumph, Gamma Medica-Ideas, Northridge, CA, USA), which was reported previously.[21] We injected 0.5 mCi (37 MBq) of ^{67}Ga-citrate in 0.1 mL of a PBS solution into each mouse through a tail vein at 8 h after exposure. SPECT images were taken at 24 h post-injection of gallium citrate. Those SPECT images were coregistered to relevant CT images and resliced as a 512 × 512 × 512 matrix. To evaluate the inflammation status, both the right and left lungs were divided into three regions (upper, middle, and lower) that were scored based on inflammation levels (1, mild inflammation and 2, moderate to severe inflammation). Scoring procedures were conducted in a blinded fashion by the chest physicians KYC and KYL who were trained by WNL and JKC. Total scores were then obtained from the summation of six regions in the lungs. More information is provided in the supplementary materials.

CT analysis

CT was performed with a preclinical tri-modality imaging system (FLEX Triumph, Gamma Medica-Ideas, Northridge, CA, USA), which was reported previously.[21] Abnormalities was evaluated on the CT images in a blinded fashion by the chest physicians KYC and KYL. More information is provided in the supplementary materials.

Inflammation, lactic dehydrogenase (LDH), and total protein in BALF

Interleukin (IL)-6, IL-10, tumor necrosis factor (TNF)-α, and interferon (IFN)-γ in BALF samples were analyzed by the BD Cytometric Bead Array tests (San Jose, CA, USA), according to the

Table 1
Sources and physical characterization of nickel oxide nanoparticles (*NiONPs*).

	Average diameter (nm)[a]	Purity (wt%)[a]	Endotoxin (EU/ml)	BET-specific surface area (m^2/g)	DLS hydrodynamic diameter (nm)	Zeta potential (mV)
NiONP	20	99.9	<0.1	7.2	685.7	−31.3

[a] Provided by the manufacturer.

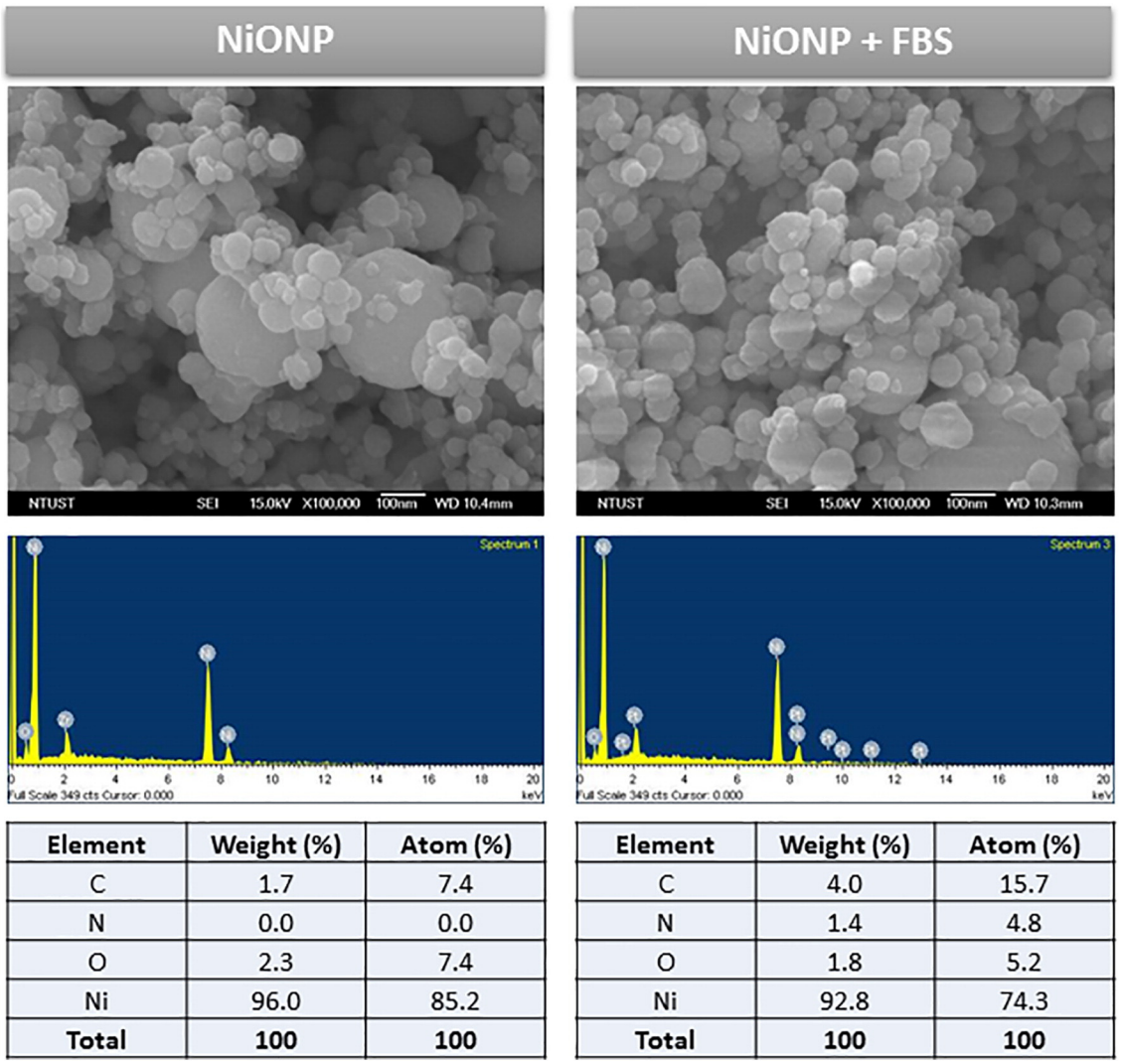

Element	Weight (%)	Atom (%)
C	1.7	7.4
N	0.0	0.0
O	2.3	7.4
Ni	96.0	85.2
Total	**100**	**100**

Element	Weight (%)	Atom (%)
C	4.0	15.7
N	1.4	4.8
O	1.8	5.2
Ni	92.8	74.3
Total	**100**	**100**

Figure 2. FE-SEM and EDX analyses of raw powdered nickel oxide nanoparticles (NiONPs) and suspended NiONPs in 5% fetal bovine serum (FBS)-containing PBS. There was no significant change in the morphology when NiONPs were suspended in FBS-containing PBS. C and N weight percents increased when NiONPs were suspended in FBS-containing PBS, whereas the O and Ni weight percents decreased.

manufacturer's instructions. Complexes of beads and proteins labeled with phycoerythrin antibodies were acquired with a BD LSRFortessa™ cell analyzer (San Jose, CA, USA). LDH and total protein were determined with an LDH cytotoxicity assay kit (Cayman, Ann Arbor, MI, USA) and a total protein assay kit (BioRad, Hercules, CA, USA), respectively, according to the manufacturers' instructions.

Enzyme-linked immunosorbent assay (ELISA) of lung tissues

For protein isolation, lung tissues were homogenized in RIPA buffer (Sigma) with Complete™ protease inhibitor (Roche Diagnostics, Basel, Switzerland), according to the manufacturers' instructions. An ELISA was used to determine 8-hydroxy-2′-deoxyguanosine (8-OHdG; Cayman) and caspase-3 activity (Millipore, Billerica, MA, USA), according to the manufacturers' instructions. Levels of these markers were adjusted to the total lung-isolated proteins.

Protein digestion and iTRAQ labeling

In the present study, lung-isolated proteins within the same group (n = 6) at 20 μg of exposure to NiONPs were pooled: 24-h control (0 μg) vs. 24-h 20 μg NiONPs (20 μg) and 28-day control

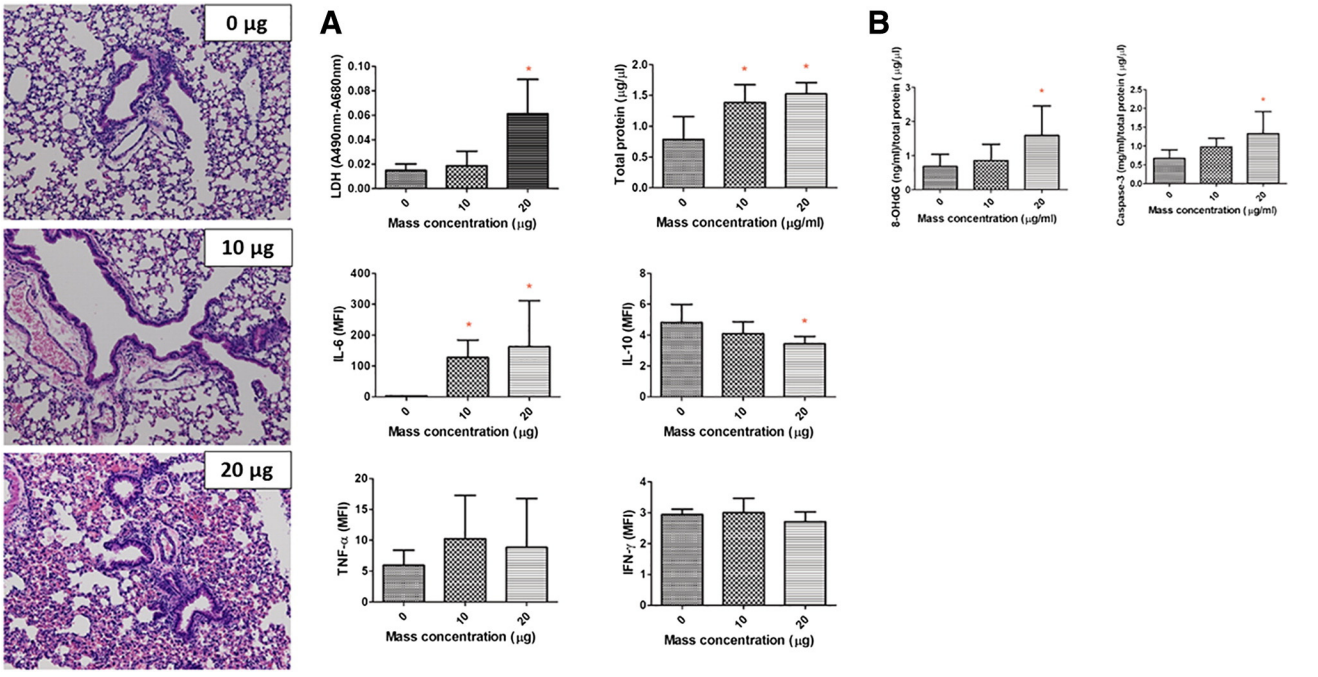

Figure 3. Acute effects of nickel oxide nanoparticles (NiONPs) on the lung inflammopathology in mice (n = 6). H&E staining of lung sections of mice with inflammatory infiltration (×400) for NiONP exposure at 0, 10, and 20 μg at 24 h. (**A**) Cytotoxic lactic dehydrogenase (LDH), total protein, inflammatory interleukin (IL)-6, IL-10, tumor necrosis factor (TNF)-α, and interferon (IFN)-γ in bronchoalveolar lavage fluid (BALF). (**B**) Oxidative stress-related 8-hydroxy-2′-deoxyguanosine (8-OHdG), and apoptotic caspase-3 in lung tissues (adjusted total protein). Significant increases in LDH, total protein, and IL-6 and a decrease in IL-10 in BALF were observed, whereas significant increases in 8-OHdG and caspase-3 were observed in lung tissues. * $P < 0.05$.

(0 μg) vs. 28-day 20 μg NiONPs (20 μg). Lung-isolated protein samples were depleted of albumin and immunoglobulin G (IgG) with a Qproteome Albumin/IgG Depletion Kit (Qiagen, Germantown, MD, USA). Protein digestion and iTRAQ labeling were previously reported.[22] More information is provided in the supplementary materials.

Liquid chromatography–tandem mass spectroscopy (LC–MS/MS)

iTRAQ-labeled protein samples were analyzed using a nano LC-Quadruple Orbitrap equipped with high-energy collision dissociation (HCD) technology, as previously reported.[23] Briefly, samples were analyzed using a Q Exactive mass spectrometer (Thermo Fisher Scientific, Bremen, Germany) coupled with an UltiMate 3000 RSLC system (Dionex, Sunnyvale, ST, USA). The criteria used for selection of differentially expressed proteins were previously reported,[24] which were (1) at least two unique high-scoring peptides in the protein; (2) $P < 0.05$ across two independent iTRAQ experiments; and (3) a protein ratio of >1.3 or <0.77. More information is provided in the supplementary materials.

Protein functional analysis

The identified upregulated and downregulated proteins in the lungs for the 24-h and 28-day groups (20 μg NiONPs) were subjected to functional pathway analyses using the Database for Annotation, Visualization and Integrated Discovery (DAVID) gene functional analytical tools (http://david.abcc.ncifcrf.gov/).[25,26] For the DAVID analysis, an enhanced score ≥ 1.3, set as the threshold, was considered to be significant, as described previously.[27]

Histology

Lungs were fixed in 10% neutral buffered formalin, embedded in paraffin, sectioned, and stained with hematoxylin and eosin (H&E). A histopathologist (CHL) examined the histological samples in a blinded fashion under light microscopy.

Data analysis

Data are presented as the mean ± standard deviation (SD), and all experiments were conducted at least three times. A one-way analysis of variance (ANOVA) with Tukey's post-hoc test was used for comparisons among multiple values. The statistical analyses were performed using GraphPad vers. 5 (CA, USA) for Microsoft Windows. The level of significance was set to $P < 0.05$.

Results

Characterization of NiONPs

Table 1 shows the physicochemical characterization of NiONPs used in this study. The average diameter of NiONPs was 20 nm with 99.9% purity of nickel. The BET surface area of the NiONPs was 7.2 m^2/g with <0.1 EU/ml endotoxin. When NiONPs were suspended in 5% FBS-containing PBS, the mean hydrodynamic diameter and zeta potential were 685.7 nm and −31.3 mV, respectively. The physicochemical characteristics of NiONPs as a raw powder and suspended in 5% FBS-containing PBS were further investigated as shown in Figure 2. Raw powder and suspended NiONPs in FBS-containing PBS were mainly spherical

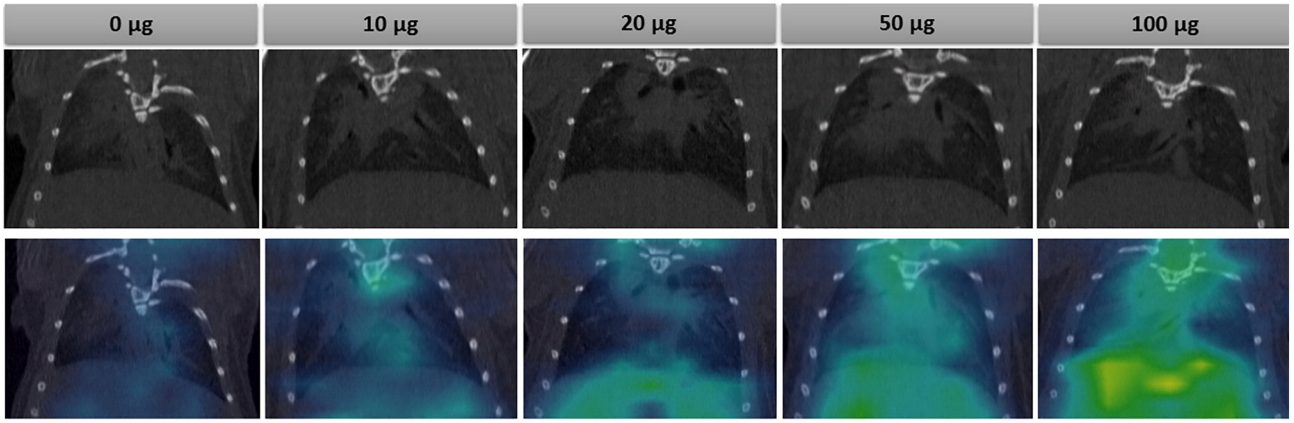

	Right	Left
Upper		
Middle		
Lower		
Total	0	

	Right	Left
Upper		++
Middle		+
Lower		++
Total	5	

	Right	Left
Upper	+	+
Middle		
Lower	++	++
Total	6	

	Right	Left
Upper	++	
Middle	+	++
Lower	++	++
Total	9	

	Right	Left
Upper	++	+
Middle	++	+
Lower	++	++
Total	10	

Figure 4. SPECT imaging analysis of lung sections at 24 h after nickel oxide nanoparticle (NiONP) exposure at 0 (PBS), 10, 20, 50, and 100 μg per mouse ($n = 1$). Both the right and left lungs were divided into three regions (upper, middle, and lower) and scored for inflammatory levels [score 1, mild inflammation (blue color); score 2, moderate to severe inflammation (green to yellow color)]. Total scores were then obtained from summation of the six regions of the lungs. Inflammation scores of the lungs are presented in a dose-dependent manner from upper to lower airways after nickel oxide nanoparticle (NiONP) exposure.

particles with aggregation. Notably, we observed that carbon (C) and nitrogen (N) weight percents increased when NiONPs were suspended in FBS-containing PBS, whereas the oxygen (O) and Ni weight percents decreased.

Pulmonary injury and inflammation in acute pulmonary effects

Figure 3 shows pulmonary injury and inflammatory responses after NiONP exposure for the 24-h follow-up experiment. LDH significantly increased with NiONP exposure at 20 μg in BALF ($P < 0.05$), whereas pulmonary total protein significantly increased with NiONP exposure at 10 and 20 μg ($P < 0.05$) (Figure 3, *A*). We also observed that the inflammatory IL-6 significantly increased with NiONP exposure at 10 and 20 μg in BALF ($P < 0.05$), whereas the anti-inflammatory IL-10 significantly decreased with NiONP exposure at 20 μg ($P < 0.05$). There was no significant difference in TNF-α or IFN-γ caused by NiONPs. H&E images showed that significant inflammatory infiltration had occurred due to NiONPs at 10 μg. In terms of lung tissues (adjusted to the total protein), oxidative stress-related 8-OHdG and apoptotic caspase-3 significantly increased with NiONP exposure at 20 μg ($P < 0.05$) (Figure 3, *B*).

SPECT analysis

SPECT was used to determine inflammatory patterns in the lungs caused by NiONPs at different concentrations (0-100 μg) after 24 h of exposure, as shown in Figure 4. We observed that inflammation scores in lungs exhibited a dose-dependent response after NiONP exposure. A severe whole-lung inflammatory response occurred with 100 μg NiONPs. Inflammatory responses occurred upon IT-administered NiONP concentrations, which mainly occurred in the upper to lower lungs upon NiONP administration.

Chest CT

NiONP-induced abnormalities of lung structures were observed over the 28 days, which included the first bronchial bifurcation, left subsegment of the secondary bronchial bifurcation, right subsegment of the secondary bronchial bifurcation, and end of the secondary bronchial bifurcation (Figure 5). First, we observed that lung parenchyma inflammation/small airway inflammation in first bronchial bifurcation occurred after 7 days of NiONP exposure. The inflammatory responses in the left subsegment of the secondary bronchial bifurcation, right subsegment of the secondary bronchial bifurcation, and end of the secondary bronchial bifurcation were mainly seen after 1 day of NiONP exposure. Together, NiNP exposure induced lung parenchyma inflammation/small airway inflammation in the left and right subsegments of the secondary bronchial bifurcation and the end of the secondary bronchial bifurcation after 1 day of exposure, whereas lung parenchyma inflammation and small airway inflammation were observed in the whole lung by NiONPs after 7 days of exposure.

Pulmonary injury and inflammation in subacute pulmonary effects

Figure 6 shows pulmonary injury and inflammatory responses after NiONP exposure for the 28-day follow-up experiment. Generally, there were no significant differences in levels of LDH, total protein, IL-6, IL-10, TNF-α, or IFN-γ at different exposure concentrations of NiONPs in BALF samples (Figure 6, *A*). We observed that 8-OHdG in lung tissues (adjusted to the total protein) significantly increased with NiONP exposure at 100 μg ($P < 0.05$) (Figure 6, *B*), but this was not observed for caspase-3. Notably, formation of pulmonary fibrosis was observed at various NiONP concentrations at 28 days.

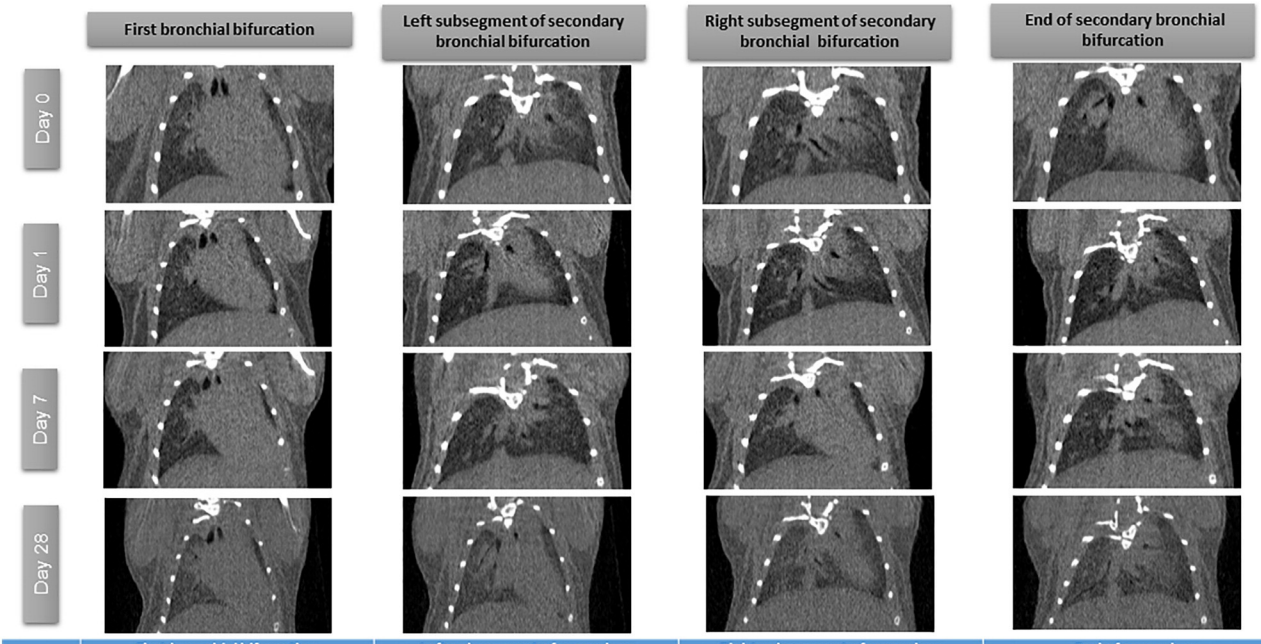

	First bronchial bifurcation					Left subsegment of secondary bronchial bifurcation					Right subsegment of secondary bronchial bifurcation					End of secondary bronchial bifurcation				
	0 μg	10μg	20μg	50μg	100μg	0 μg	10μg	20μg	50μg	100μg	0 μg	10μg	20μg	50μg	100μg	0 μg	10μg	20μg	50μg	100μg
0 day	0/6	0/6	0/6	1/6	0/6	0/6	0/6	1/6	2/6	1/6	0/6	0/6	2/6	2/6	2/6	0/6	0/6	2/6	2/6	1/6
1 day	0/6	2/6	2/6	4/6	2/6	0/6	2/6	3/6	5/6	5/6	1/6	2/6	3/6	4/6	3/6	1/6	2/6	1/6	6/6	3/6
7 day	1/6	3/6	3/6	3/6	1/6	1/6	4/6	3/6	4/6	3/6	0/6	1/6	3/6	4/6	2/6	1/6	1/6	3/6	4/6	3/6
28 day	1/6	4/6	5/6	3/6	6/6	2/6	5/6	5/6	3/6	6/6	1/6	6/6	5/6	6/6	5/6	1/6	6/6	5/6	5/6	6/6

Figure 5. Chest CT imaging analysis at 0, 1, 7, and 28 days after nickel oxide nanoparticle (NiONP) exposure at 100 μg by intratracheal (IT) instillation (n = 6). Four sections of the chest CT were observed: first bronchial bifurcation, left subsegment of the secondary bronchial bifurcation, right subsegment of the secondary bronchial bifurcation, and the end of the secondary bronchial bifurcation. Lung parenchyma inflammation and small airway inflammation were identified from the first bronchial bifurcation to the end of the secondary bronchial bifurcation with different exposure concentrations and times. Yellow highlighting indicates that more than half of the mice were observed to have lung parenchyma inflammation/small airway inflammation.

Protein expressions and 24-h and 28-day pathways after exposure

Totals of 304 and 246 proteins were respectively identified for the 24-h and 28-day periods after NiONP exposure, among which 212 and 141 proteins were quantified as iTRAQ-labeled samples, respectively. We then selected differentially expressed proteins based on the three criteria mentioned in "Materials and methods", which included 139 proteins for 24-h follow-up and 26 proteins for 28-day follow-up of exposure. These proteins are listed in Supplementary Information. The 24-h expressed proteins were involved in 12 pathways, and seven of these were identified to be significant (Figure 7). These included focal adhesion, *Vibrio cholerae* infection, endocytosis, drug metabolism by cytochrome P450, biosynthesis of amino acids, hypertrophic cardiomyopathy, and salmonella infection. The 28-day expressed proteins were involved in four pathways, and two of these were identified to be significant (Figure 7), including glutathione metabolism and metabolism of xenobiotics by cytochrome P450.

Discussion

In this study, the pulmonary inflammopathology of exposure to NiONPs was investigated in mice. There are four major findings reported in the present study: (1) exposure to NiONPs induced dose-dependent acute lung injury, upper-to-lower airway inflammation, oxidative stress, and caspase-3 at 24 h of exposure; (2) lung parenchyma inflammation and small airway inflammation were induced by NiONPs after exposure from the left and right subsegments and end of the secondary bronchial bifurcation to the whole lungs; (3) oxidative stress was persistent with pulmonary fibrosis observed at 28 days after NiONP exposure; and (4) distinct pathways were activated by NiONPs at 24 h and 28 days of exposure.

Surfactants are commonly used to disperse NPs and reduce NP aggregation/agglomeration in biological solutions. Serum proteins, for example, were reported to adequately disperse NPs with negligible negative effects in biological systems.[28,29] Also, our previous study indicated that there was no significant difference of oxidative stress and inflammatory responses caused by serum protein.[30] In the present study, we observed that a higher weight percentage of N was detected in spherical NiONPs after being suspended in FBS-containing PBS, suggesting that a small amount of serum protein may have adhered/interacted with the surface of NiONPs. When NiONPs are inhaled into the lung environment, epithelial lining fluid is able to provide an abundance of surfactant proteins to interact with NiONPs. Therefore, levels of NiONP re-aggregation may be insignificant after IT administration after a certain period, but more evidence should be provided to support this hypothesis.

Acute (24 h) and subacute pulmonary inflammatory effects (28 days) after a single IT instillation of NiONPs were investigated in

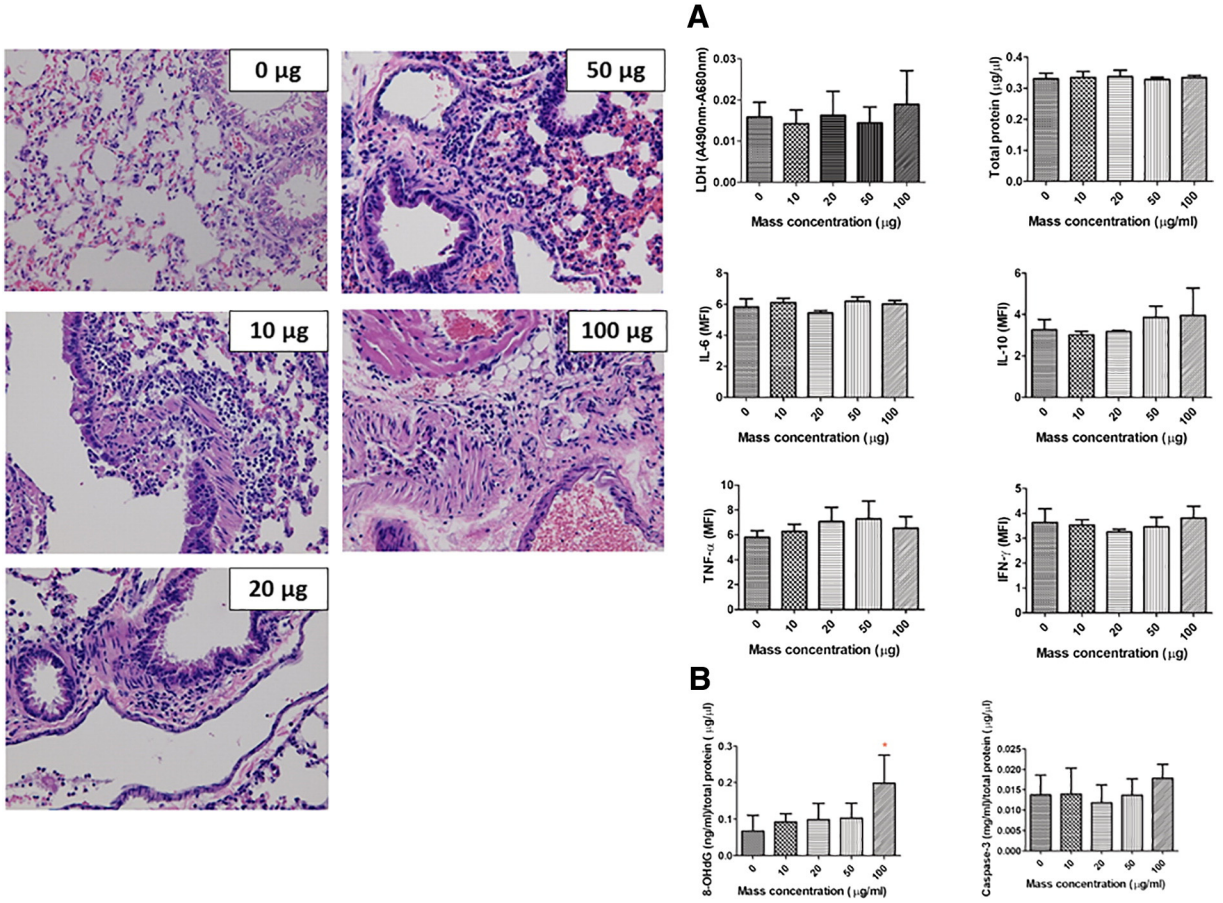

Figure 6. Subacute effects of nickel oxide nanoparticles (NiONPs) on the lung inflammopathology in mice ($n = 6$). H&E staining of lung sections (×400) with fibrosis for NiONP exposure at 10, 20, 50, and 100 μg in mice at 28 days. (**A**) Cytotoxic lactic dehydrogenase (LDH), total protein, inflammatory interleukin (IL)-6, IL-10, tumor necrosis factor (TNF)-α, and interferon (IFN)-γ in bronchoalveolar lavage fluid (BALF). (**B**) Oxidative stress-related 8-hydroxy-2′-deoxyguanosine (8-OHdG), and apoptotic caspase-3 in lung tissues (adjusted total protein). There was a significant increase in 8-OHdG in lung tissues. $^*P < 0.05$.

mice. The rationale for NiONP administration was based on a previous report.[17] Mass concentrations applied in the present study were relevant to occupational exposure scenarios in humans,[18] including the alveolar surface area, breathing frequency, and lung deposition rate. Also, occupational environmental conditions were considered such as working day ventilation and permissible exposure limits for nickel. In the present study, the human-equivalent NiONP mass concentrations were achieved at 6.8 days for 10 μg, 13.6 days for 20 μg, 34 days for 50 μg, and 68 days for 100 μg. To investigate NiONP's effects on the pulmonary system, we selected 20 μg as the highest concentration for IT administration. The reasons were as follows: (1) 20 μg of NiONPs is able to induce a significant oxidative–inflammatory response in the lungs without significant lung injury such as alveolar destruction, and (2) this dose is relevant to 13.6 days of a human-equivalent mass concentration. For the subacute response, the maximum dose (i.e., 100 μg) following IT instillation may be close to the lung burden in subacute inhalation exposure of NiONPs under the same experimental conditions as in the present study.

To investigate the inflammopathology caused by NiONPs, we first compared pulmonary inflammation at 24 h after exposure to NiONPs between the BALF and lung tissues. In BALF samples, exposure to NiONPs increased the cytotoxic LDH and pulmonary permeability total protein accompanied by an increase of IL-6 and a decrease of IL-10. These findings were in accordance with recent in vivo studies on various metal oxide NPs.[31-33] Oxidative stress and reactive oxygen species (ROS) formation are related to NiONP exposure and are associated with different biological effects that depend on the physicochemistry of NiONPs. For example, NiONPs are able to release Ni^{2+} in the dispersion and lung environment,[34] leading to oxidative disruption. Indeed, we found that the oxidative stress-related 8-OHdG and apoptotic caspase-3 significantly increased due to NiONPs in mice lungs. ROS are reactive molecular species with an unpaired electron in their outer orbit,[35,36] which is able to interact with surrounding molecules by redox reactions. Accumulation of ROS produced by NiONPs in the lung environment can continuously damage cells causing DNA lesions, with the consequence of cell death such as by apoptosis. Inflammation is a protective response, which involves an influx of inflammatory cells to the lung. This transient response can lead to a second wave of oxidative stress, since activated inflammatory cells also generate and release significant quantities of free radicals,[37] leading to a secondary inflammatory response.

Based on biochemical results obtained from the BALF and lung tissues, we know that NiONP exposure is able to induce acute oxidative–inflammatory reactions and activate cell apoptosis.

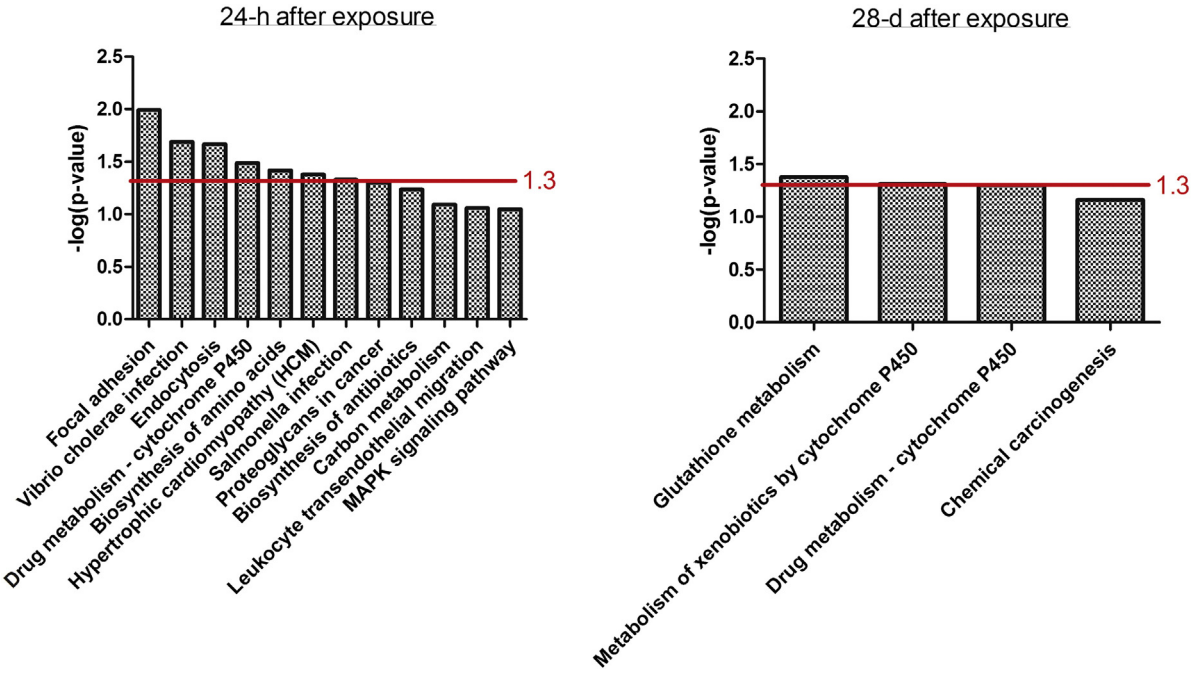

Figure 7. Pathways associated with the downregulation and upregulation of lung protein responses at 24 h and 28 days after exposure to nickel oxide nanoparticles (NiONPs) were determined using a DAVID analysis. An enhanced score [−log(*P* value)] ≥1.3 threshold (red line) was considered to be significant. Focal adhesion, *Vibrio cholerae* infection, endocytosis, drug metabolism by cytochrome P450, biosynthesis of amino acids, hypertrophic cardiomyopathy, and salmonella infection were identified as significant pathways in the 24-h response to NiONPs. Glutathione metabolism and metabolism of xenobiotics by cytochrome P450 were identified as significant pathways in the 28-day response to NiONPs.

However, the progression of lung inflammation remains unclear. To get a better picture of acute lung inflammation, SPECT was first applied to investigate dose-dependent resolution of NiONP-induced lung inflammation. SPECT images showed inflammation from the upper to the lower airways by NiONPs in a dose-dependent manner. The highest concentration of NiONPs (100 μg) caused a severe whole-lung inflammatory response. Notably, a distinct inflammatory pattern was observed after administration of NiONPs via IT instillation. For example, IT administration of 10 μg NiONPs mainly caused tracheal and upper airway inflammation. Whole-lung inflammation occurred when >50 μg of NiONPs was administered. Additionally, we found that SPECT images were in accordance with the biochemical results.

To investigate the pathological progression over the 28 days after NiONP exposure, chest CT was used to increase the time-dependent resolution. We divided lung images into four sections, including the first bronchial bifurcation, left subsegment of the secondary bronchial bifurcation, right subsegment of the secondary bronchial bifurcation, and the end of the secondary bronchial bifurcation. Lung parenchyma inflammation and small airway inflammation were mainly identified in the lungs by NiONPs. Chest CT results indicated a dose-dependent and time-dependent progression of lung parenchyma inflammation/small airway inflammation caused by NiONPs over 28 days. For example, inflammation was mainly observed in the end of the secondary bronchial bifurcation with higher concentrations (50 and 150 μg) of NiONPs. Lung parenchyma inflammation/small airway inflammation in the first bronchial bifurcation mainly occurred after 7 days of NiONP exposure. Notably, we observed that the left and right subsegments of the secondary bronchial bifurcation were important target regions of NiONPs, where lung parenchyma inflammation/small airway inflammation was observed after 1 day of exposure at various NiONP concentrations.

By comparing inflammatory features, similar results were observed between SPECT and CT images with 24-h exposure. The chest CT further identified the pathological occurrence and structural changes due to NiONP exposure. As the increasing number of bifurcations in the tracheobronchial region leads to a fall in air/liquid velocity, NiONPs may be delivered to and accumulate in the alveolar zone of the distal respiratory tract. These accumulating NiONPs are either captured by macrophages or even translocated into the circulation. Notably, we did not observe significant alterations in the cytotoxic LDH, permeability total protein, or inflammation in BALF or apoptotic caspase-3 in lung tissues, but oxidative stress-related 8-OHdG did change. These results are in line with previous findings in Sprague–Dawley rats,[16] suggesting that inflammatory responses had been mitigated or eliminated in the lungs by 28 days after IT instillation of NiONPs. Pulmonary exposure to NiONPs provoked an acute inflammatory response, followed by a secondary systemic inflammatory response.[16] Secondary inflammation might not have persisted in the lungs over 28 days after exposure, or inflammation might be observed at lower levels. Importantly, we observed formation of fibrosis in the lungs at 28 days after exposure to various concentrations of NiONPs. Pulmonary fibrosis was also previously observed by metal-based oxide NPs.[38] Chronic pulmonary fibrosis with low-grade inflammation was reported previously,[39] which is in line with chest CT findings of

the present study. The lung parenchyma inflammation/small airway inflammation may progress to fibrotic stages at 28 days after NiONP exposure. Therefore, initiation of pulmonary fibrosis could be an important pathological change with NiONP exposure.

Next, we used an iTRAQ-coupled LC–MS/MS approach to discover the underlying pathways in lung tissues after 24 h and 28 days of NiONP exposure. Proteomic techniques are widely applied in clinical and biological investigations,[40,41] and provide comprehensive information with which to understand biological networks. We found that focal adhesion, *Vibrio cholerae* infection, endocytosis, drug metabolism by cytochrome P450, biosynthesis of amino acids, hypertrophic cardiomyopathy, and salmonella infection were important pathways in the 24-h response to NiONPs. Enhanced adhesive signaling, including activation of a focal adhesion kinase, is a hallmark of fibroblasts from pulmonary fibrosis patients, and focal adhesion kinase is therefore considered a key mediator of pulmonary fibrosis.[42] Activation of a focal adhesion kinase after 24 h of NiONP exposure may be a critical mechanism in initiating pulmonary fibrosis in mice as fibrosis was observed in lungs at 28 days after NiONP exposure. Additionally, endocytosis was also observed in the 24-h response to NiONPs, which was reported to be an essential biological response to phagocytosis of NPs.[43] Clearance of NiONPs from the lung environments depends on their physicochemistry such as size, shape, and surface characteristics.[44] Only two pathways were identified at 28 days in the present study, including glutathione metabolism and metabolism of xenobiotics by cytochrome P450. It is predictable that pulmonary effects caused by NiONP exposure would have recovered to a normal status by 28 days after exposure, but glutathione metabolism was still activated in the lungs, which may explain the observation of increased 8-OHdG in lung tissues at 28 days after exposure. The chronic oxidative imbalance is also implicated as an important molecular mechanism underlying fibrosis in the lungs.[45]

There are some limitations to the present study. Due to the radiative issue and reduction of animal use, only one mouse was randomly selected per group for the SPECT analysis to limit radiation exposure. More mice should be used in future work. Although exposure to NiONP concentrations was estimated based on previous reports, a single IT instillation at a high concentration could lead to acute lung injury/damage. The Ni levels in the lungs should be examined to understand the possible effects of NiNP after exposure. Pulmonary fibrosis was observed in the present study, and the underlying mechanism should be investigated in future work.

In conclusion, comprehensive approaches, from image analyses to proteomics, were used to investigate the effects of NiONP exposure on the pulmonary inflammopathology in mice. Acute upper-to-lower lung inflammation occurred at 24 h after NiONP exposure, which was accompanied by oxidative stress-related 8-OHdG and apoptotic caspase-3. Lung parenchyma inflammation and small-airway inflammation were observed in lungs by NiONPs over 28 days of exposure with increased oxidative stress. Pulmonary fibrosis and its related pathway of focal adhesion were identified, with the latter having been activated at 24 h after NiONP exposure. With the image analysis (e.g. CT and SPECT), real-time inflammopathology caused by nanoparticles can be evaluated in rodent, which provides more accurate information for nanotoxicology.

Authors' Contributions

KJB, KJC and HCC contributed to the completion of interpretation of the data and the manuscript. **HCC** contributed substantially to the concept, the design, interpretation of the data and the completion of the study and the manuscript. **JKC** and **WNL** contributed to the SPECT and CT analyses. **HEH** and **YLS** contributed substantially to the completion of the study. **CHL**, **KYC** and **KYL** contributed to the interpretation of the pathology, SPECT and CT data. **TCH, CHP and KFH** contributed to the physical characterization of nanoparticles. All authors contributed to the critically revising the manuscript for important intellectual content. All authors have read and approved the final manuscript.

Acknowledgment

Authors heartedly thank Miss Yi-Syuan Lin for technical assistance during this project. Authors are grateful for the animal care support provided by Mr. Chien-Hung Chen and radio-technical support from Miss Sih-Yu Chen (NM-104-PP-27).

Appendix A. Supplementary data

The materials and methods and data of protein list are presented in Supplementary Information. Supplementary data associated with this article can be found in the online version, at https://doi.org/10.1016/j.nano.2017.10.003.

References

1. Denkhaus E, Salnikow K. Nickel essentiality, toxicity, and carcinogenicity. *Crit Rev Oncol Hematol* 2002;**42**:35-56.
2. National Toxicology, P. NTP toxicology and carcinogenesis studies of nickel oxide (CAS no. 1313-99-1) in F344 rats and B6C3F1 mice (inhalation studies). *Natl Toxicol Program Tech Rep Ser* 1996;**451**:1-381.
3. IARC. *IARC Monographs on the Evaluation of Carcinogenic Risks to Humans, Volume 49: Chromium, Nickel and Welding*; 1990.
4. Magaye R, Zhao J. Recent progress in studies of metallic nickel and nickel-based nanoparticles' genotoxicity and carcinogenicity. *Environ Toxicol Pharmacol* 2012;**34**:644-50.
5. Mu Y, Jia D, He Y, Miao Y, Wu HL. Nano nickel oxide modified non-enzymatic glucose sensors with enhanced sensitivity through an electrochemical process strategy at high potential. *Biosens Bioelectron* 2011;**26**:2948-52.
6. Squadrito GL, Cueto R, Dellinger B, Pryor WA. Quinoid redox cycling as a mechanism for sustained free radical generation by inhaled airborne particulate matter. *Free Radic Biol Med* 2001;**31**:1132-8.
7. Levitzky M. *Pulmonary Physiology*. McGraw-Hill; 2007.
8. Nemmar A, Hoet PH, Vanquickenborne B, Dinsdale D, Thomeer M, Hoylaerts MF, et al. Passage of inhaled particles into the blood circulation in humans. *Circulation* 2002;**105**:411-4.
9. Donaldson K, Stone V, Seaton A, MacNee W. Ambient particle inhalation and the cardiovascular system: potential mechanisms. *Environ Health Perspect* 2001;**109**(Suppl 4):523-7.
10. Cho WS, Duffin R, Poland CA, Duschl A, Oostingh GJ, Macnee W, et al. Differential pro-inflammatory effects of metal oxide nanoparticles and their soluble ions in vitro and in vivo; zinc and copper nanoparticles, but not their ions, recruit eosinophils to the lungs. *Nanotoxicology* 2012;**6**:22-35.
11. Cho WS, Duffin R, Poland CA, Howie SE, MacNee W, Bradley M, et al. Metal oxide nanoparticles induce unique inflammatory footprints in the

lung: important implications for nanoparticle testing. *Environ Health Perspect* 2010;**118**:1699-706.
12. Larsen GL, Holt PG. The concept of airway inflammation. *Am J Respir Crit Care Med* 2000;**162**:S2-6.
13. Ogami A, Morimoto Y, Myojo T, Oyabu T, Murakami M, Todoroki M, et al. Pathological features of different sizes of nickel oxide following intratracheal instillation in rats. *Inhal Toxicol* 2009;**21**:812-8.
14. Qian F, He M, Duan W, Mao L, Li Q, Yu Z, et al. Cross regulation between hypoxia-inducible transcription factor-1alpha (HIF-1alpha) and transforming growth factor (TGF)-ss1 mediates nickel oxide nanoparticles (NiONPs)-induced pulmonary fibrosis. *Am J Transl Res* 2015;**7**:2364-78.
15. Ye H, Sun L, Huang X, Zhang P, Zhao X. A proteomic approach for plasma biomarker discovery with 8-plex iTRAQ labeling and SCX-LC-MS/MS. *Mol Cell Biochem* 2010;**343**:91-9.
16. Chuang HC, Juan HT, Chang CN, Yan YH, Yuan TH, Wang JS, et al. Cardiopulmonary toxicity of pulmonary exposure to occupationally relevant zinc oxide nanoparticles. *Nanotoxicology* 2014;**8**:593-604.
17. Vietti G, Ibouraadaten S, Palmai-Pallag M, Yakoub Y, Bailly C, Fenoglio I, et al. Towards predicting the lung fibrogenic activity of nanomaterials: experimental validation of an in vitro fibroblast proliferation assay. *Part Fibre Toxicol* 2013;**10**:52.
18. Rovira E, Cuadras A, Aguilar X, Esteban L, Borras-Santos A, Zock JP, et al. Asthma, respiratory symptoms and lung function in children living near a petrochemical site. *Environ Res* 2014;**133**:156-63.
19. Galer DM, Leung HW, Sussman RG, Trzos RJ. Scientific and practical considerations for the development of occupational exposure limits (OELs) for chemical substances. *Regul Toxicol Pharmacol* 1992;**15**:291-306.
20. OSHA. *Occupational Health Guideline for Nickel Metal and Soluble Nickel Compounds*. Occupational Safety and Health Administration; 1978.
21. Chuang HC, Chuang KJ, Chen JK, Hua HE, Shen YL, Liao WN, et al. Pulmonary pathobiology induced by zinc oxide nanoparticles in mice: a 24-hour and 28-day follow-up study. *Toxicol Appl Pharmacol* 2017;**327**:13-22.
22. Chuang K-J, Pan C-H, Su C-L, Lai C-H, Lin W-Y, Ma C-M, et al. Urinary neutrophil gelatinase-associated lipocalin is associated with heavy metal exposure in welding workers. *Sci Rep* 2015;**5**:18048.
23. Boja ES, Phillips D, French SA, Harris RA, Balaban RS. Quantitative mitochondrial phosphoproteomics using iTRAQ on an LTQ-Orbitrap with high energy collision dissociation. *J Proteome Res* 2009;**8**:4665-75.
24. Ruppen I, Grau L, Orenes-Pinero E, Ashman K, Gil M, Algaba F, et al. Differential protein expression profiling by iTRAQ-two-dimensional LC-MS/MS of human bladder cancer EJ138 cells transfected with the metastasis suppressor KiSS-1 gene. *Mol Cell Proteomics* 2010;**9**:2276-91.
25. Huang da W, Sherman BT, Tan Q, Kir J, Liu D, Bryant D, et al. DAVID bioinformatics resources: expanded annotation database and novel algorithms to better extract biology from large gene lists. *Nucleic Acids Res* 2007;**35**:W169-175.
26. Srivastava R, Ray S, Vaibhav V, Gollapalli K, Jhaveri T, Taur S, et al. Serum profiling of leptospirosis patients to investigate proteomic alterations. *J Proteomics* 2012;**76**:56-68.
27. Huang da W, Sherman BT, Lempicki RA. Systematic and integrative analysis of large gene lists using DAVID bioinformatics resources. *Nat Protoc* 2009;**4**:44-57.
28. Wells MA, Abid A, Kennedy IM, Barakat AI. Serum proteins prevent aggregation of Fe2O3 and ZnO nanoparticles. *Nanotoxicology* 2012;**6**:837-46.
29. Zook JM, Maccuspie RI, Locascio LE, Halter MD, Elliott JT. Stable nanoparticle aggregates/agglomerates of different sizes and the effect of their size on hemolytic cytotoxicity. *Nanotoxicology* 2011;**5**:517-30.
30. Chiang LL, Chen HC, Lee CN, Chuang KJ, Chen TT, Yeh CT, et al. Serum protein oxidation by diesel exhaust particles: effects on oxidative stress and inflammatory response in vitro. *Chem Biol Interact* 2013;**206**:385-93.
31. Teeguarden JG, Mikheev VB, Minard KR, Forsythe WC, Wang W, Sharma G, et al. Comparative iron oxide nanoparticle cellular dosimetry and response in mice by the inhalation and liquid cell culture exposure routes. *Part Fibre Toxicol* 2014;**11**:46.
32. Demokritou P, Gass S, Pyrgiotakis G, Cohen JM, Goldsmith W, McKinney W, et al. An in vivo and in vitro toxicological characterisation of realistic nanoscale CeO(2) inhalation exposures. *Nanotoxicology* 2013;**7**:1338-50.
33. Sager T, Wolfarth M, Keane M, Porter D, Castranova V, Holian A. Effects of nickel-oxide nanoparticle pre-exposure dispersion status on bioactivity in the mouse lung. *Nanotoxicology* 2016;**10**:151-61.
34. Horie M, Fukui H, Endoh S, Maru J, Miyauchi A, Shichiri M, et al. Comparison of acute oxidative stress on rat lung induced by nano and fine-scale, soluble and insoluble metal oxide particles: NiO and TiO2. *Inhal Toxicol* 2012;**24**:391-400.
35. Novo E, Parola M. Redox mechanisms in hepatic chronic wound healing and fibrogenesis. *Fibrogenesis Tissue Repair* 2008;**1**:5.
36. Halliwell B, Gutteridge J. *Free Radicals in Biology and Medicine*. Oxford University Press; 1999.
37. Kelly FJ. Oxidative stress: its role in air pollution and adverse health effects. *Occup Environ Med* 2003;**60**:612-6.
38. Ma J, Bishoff B, Mercer RR, Barger M, Schwegler-Berry D, Castranova V. Role of epithelial-mesenchymal transition (EMT) and fibroblast function in cerium oxide nanoparticles-induced lung fibrosis. *Toxicol Appl Pharmacol* 2017;**323**:16-25.
39. Richter K, Kietzmann T. Reactive oxygen species and fibrosis: further evidence of a significant liaison. *Cell Tissue Res* 2016;**365**:591-605.
40. Ahamed M, Alhadlaq HA. Nickel nanoparticle-induced dose-dependent cyto-genotoxicity in human breast carcinoma MCF-7 cells. *Onco Targets Ther* 2014;**7**:269-80.
41. Haenen S, Clynen E, Nemery B, Hoet PHM, Vanoirbeek JAJ. Biomarker discovery in asthma and COPD: application of proteomics techniques in human and mice. *EuPA Open Proteom* 2014;**4**:101-12.
42. Lagares D, Busnadiego O, Garcia-Fernandez RA, Kapoor M, Liu S, Carter DE, et al. Inhibition of focal adhesion kinase prevents experimental lung fibrosis and myofibroblast formation. *Arthritis Rheum* 2012;**64**:1653-64.
43. Munoz A, Costa M. Elucidating the mechanisms of nickel compound uptake: a review of particulate and nano-nickel endocytosis and toxicity. *Toxicol Appl Pharmacol* 2012;**260**:1-16.
44. Mailander V, Landfester K. Interaction of nanoparticles with cells. *Biomacromolecules* 2009;**10**:2379-400.
45. Cheresh P, Kim SJ, Tulasiram S, Kamp DW. Oxidative stress and pulmonary fibrosis. *Biochim Biophys Acta* 1832;**2013**:1028-40.